LAWRENCE LIVERMORE NATIONAL LABORATORY

UCRL-CONF-205119

Deformation and Shear Band Development in an Ultrahigh Carbon Steel During High Strain Rate Deformation

Don Lesuer, Chol Syn and Oleg Sherby

July 9, 2004

Fall TMS Meeting
New Orleans, LA
September 26 – 29, 2004

This document was prepared as an account of work sponsored by an agency of the United States Government. Neither the United States Government nor the University of California nor any of their employees, makes any warranty, express or implied, or assumes any legal liability or responsibility for the accuracy, completeness, or usefulness of any information, apparatus, product, or process disclosed, or represents that its use would not infringe privately owned rights. Reference herein to any specific commercial product, process, or service by trade name, trademark, manufacturer, or otherwise, does not necessarily constitute or imply its endorsement, recommendation, or favoring by the United States Government or the University of California. The views and opinions of authors expressed herein do not necessarily state or reflect those of the United States Government or the University of California, and shall not be used for advertising or product endorsement purposes.

Deformation and Shear Band Development in an Ultrahigh Carbon Steel During High Strain Rate Deformation

Don Lesuer[1], Chol Syn[1] and Oleg Sherby[2]

[1] Lawrence Livermore National Laboratory, Livermore, CA 94551, USA
[2] Stanford University, Stanford, CA 94305, USA

Keywords: Ultrahigh carbon steel, high rate deformation, shear bands

Abstract

The mechanical response of a pearlitic UHCS-1.3C steel deformed at approximately 4000 s^{-1} to large strains (ε = -0.9) has been studied. Failure, at both the macroscopic and the microscopic levels has been evaluated, and the ability of the material to absorb energy in compression has been examined. Failure occurred by the development of a shear band. However before failure, extensive buckling of the carbide plates was observed and the UHCS-1.3C material exhibited significant potential for compressive ductility and energy absorption due to the distributed buckling of these plates. Strain localization during adiabatic shear band development resulted in the formation of austenite. Subsequent cooling produced a divorced-eutectoid transformation with associated deformation, which resulted in a microstructure consisting of 50 to 100 nm sized grains. The stress-strain behavior within the shear band has also been determined. The results are used to critically evaluate the maximum shear stress criterion of shear band development. New criteria for the development of shear bands are developed based on a strain energy concept.

Introduction

Many of the potential applications for ultrahigh carbon steels (UHCS), including products in the automotive and military sectors, involve loading at high strain rates with the potential for large strain deformation. The stress-strain and fracture response of UHCS at quasi-static strain rates has been well documented in the literature and the processing-structure-properties relationships have been reasonably well established under these conditions [1-4]. However, the response of UHCS at high strain rates has been largely unexplored [5]. In this paper, we report on a study concerning the mechanical response of a pearlitic UHCS-1.3C steel deformed at strain rates of approximately 4000 s^{-1} in compression to large strains (ε = -0.9). The ability of the material to absorb energy in compression has also been evaluated. Failure in many materials, including steels, is often the result of shear band development [6]. The results of this study have been used to evaluate the stress-strain behavior in a shear band and for critical assessment of the generally accepted criterion for shear band development (maximum shear stress criterion). This analysis has led to the development of new criteria for the development of shear bands.

Materials and Experiments

Materials and processing

The UHCS for this study had the composition 1.3%C, 3.0%Si, 0.5%Mn, 0.99%Cr and balance iron. A thirty-kilogram ingot was cast using vacuum induction melting and forged at 1090°C from a square cross-section, 125 mm wide, to a plate 25 mm thick by 100 mm wide. The resulting microstructure had small discontinuous graphite stringers induced by the graphitizing influence of silicon. After forging, the plate was homogenized for one hour at 1125°C and air-cooled. This treatment produced a fully pearlitic structure with a reduced amount of rod-shaped graphite stringers that were oriented in the longitudinal direction of the plate. This fully pearlitic structure had a hardness of VHN = 355 (R_c = 36).

Compression samples were prepared in the form of right circular cylinders, 6.35 mm in diameter and 6.35 mm tall. All samples were deformed in the longitudinal direction. Samples were prepared for study in the pearlitic and martensitic condition. The samples with a martensitic microstructure were prepared in two conditions, quenched and quenched-and-tempered. The quenched state was obtained by heating the pearlite structure plate to 880°C for 20 minutes and water quenching. The hardness of the quenched sample was VHN = 770 (R_c = 63). The quenched-and-tempered state was obtained by tempering the quenched sample at 320°C for 30 minutes followed by air-cooling. The tempered sample had a VHN = 782 (R_c = 63.5).

Experiments

Dynamic compression tests were performed using the split Hopkinson pressure bar technique. The steel sample was placed between two long bars made of Ti-6Al-4V. A striker bar is propelled toward one of the pressure bars (the input bar). Upon impact, an elastic stress wave is introduced into the input bar. This stress wave travels down the bar and at the specimen-bar interface, a portion of this wave is transferred into the sample, causing the sample to deform. The strain histories for the incident and transmitted waves in the elastic pressure bars were measured and analyzed to determine the engineering stress, engineering strain and engineering strain rate response of the sample.

Dynamic Stress-Strain Response

The dynamic mechanical response of the pearlitic UHCS, plotted as engineering stress versus engineering strain and true stress versus true strain, is shown in Fig. 1. The strain rate during testing was 4100 s^{-1}. The pearlitic UHCS showed high compression ductility. The load began to decrease precipitously at about -0.55 engineering strain and was terminated by a ring stop that limited the strain to –0.60.

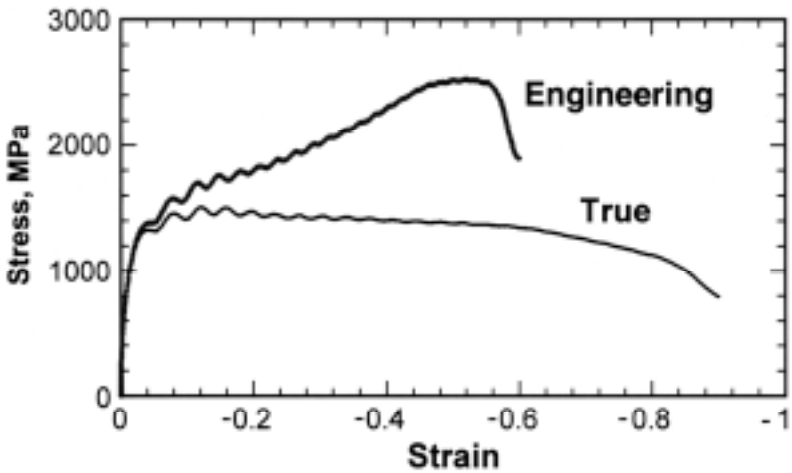

Figure 1. Stress-strain behavior in compression for pearlitic UHCS-1.3C. Results are plotted as true stress versus true strain and engineering stress versus engineering strain.

All samples failed by the initiation and propagation of adiabatic shear bands. Compression tests were repeated and the tests confirmed the reproducibility of the results. The increase in temperature during deformation up to the maximum stress was estimated by assuming that all the plastic work of deformation was converted to heat. The calculations yielded a temperature rise of 300°C for the pearlitic material.

Figure 2 shows the initial and deformed states of the pearlitic UHCS sample. The cross-section of the undeformed sample is given in Fig 2 (a). The matrix consists of a structure of fine pearlite containing a small amount of minute vertical graphite stringers. The stringers are oriented parallel to the lengthening direction during prior forging. Figure 2 (b) shows a cross-section of the deformed pearlitic sample illustrating the two adiabatic shear bands oriented at about 45° to the compression axis. The deformed sample remained intact because of the ring stopper. Discontinuous cracks are observed within the two shear bands. The adiabatic shear-band widths were measured by optical microscopy of polished-and-etched samples. The shear band width was 14 μm for the pearlitic UHCS.

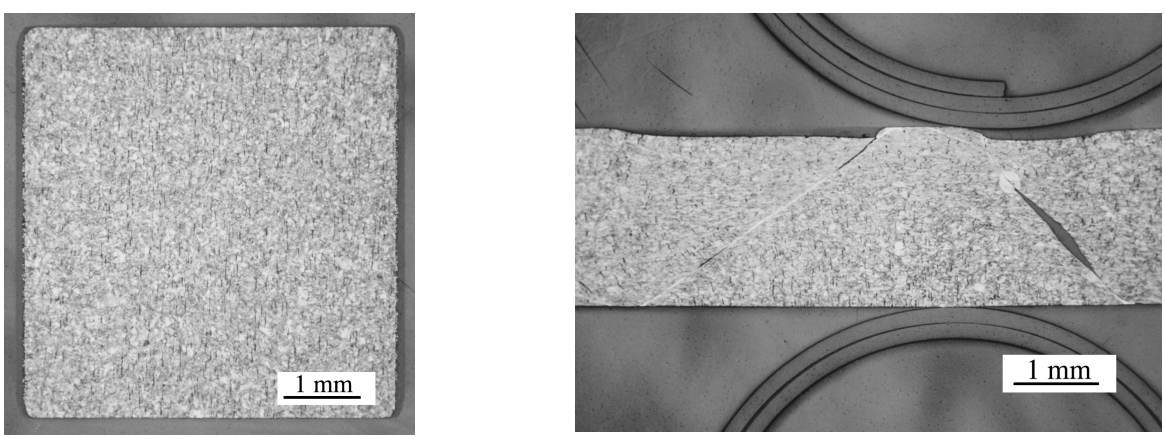

(a) (b)

Figure 2. Cross-section of the UHCS-1.3C samples before (a) and after (b) testing to 60% deformation.

An estimate can be calculated of the strain in the band from an observation of the offset of the shear band shown in Figure 2 (b). The left-hand section of the deformed sample is displaced from the center section, with a length difference of 0.125 mm along the shear line. A shear strain, γ, in the band is estimated by dividing this displacement by the shear band width (14 μm) yielding $\gamma = 11$. The calculated true strain (Von Mises) in the shear band is $\varepsilon = -6.4$. The total true strain in the band is - 6.4 plus the strain prior to the start of shear banding ($\varepsilon = -0.8$) yielding $\varepsilon = -7.2$. This true strain value is similar to those estimated for shear bands in other Fe-C materials [7-9]. The strain rate in the shear band is estimated as follows. The axial strain during shear banding is 0.044 (the axial displacement of 0.125 mm divided by the sample height of 2.86 mm), giving a time of shear banding of 1.1×10^{-5} s (0.044 divided by 4000). Thus the strain rate in the shear band is the strain in the band (6.4) divided by the deformation time in the band yielding a strain rate of 6×10^{5} s^{-1}. Such a strain rate is often quoted in studies of high velocity projectiles and high explosive charges [10]

Energy Absorption and Failure

Energy Absorption

During dynamic deformation prior to failure, the pearlitic sample showed enormous potential for absorbing energy. Figures 3a and 3b show the pearlitic sample after deformation to engineering strains of 0.30 and 0.60 respectively. The figures show pronounced kinking of the carbide plates. The kinking is much more extensive in the sample deformed to 0.60 strain than the sample deformed to 0.30. In both samples the kinking and multiple shearing is highly distributed throughout the sample. This distributed kinking can absorb significant amounts of energy during deformation of the pearlitic UHCS material. Figure 4 shows a region in the pearlitic sample deformed to e = 0.60 in which intense local shear was observed. The dominant shear band in the center of the micrograph in Fig. 4a is about 0.5 μm in width. Other shear bands in the figure are smaller but the spacing between bands is about 1 μm. As clearly shown in Fig. 4b, the carbide plates in these bands are continuous and don't show any obvious fractures. It is important to note that these bands are significantly smaller in size than the 14 μm major shear band that was associated with the loss in load bearing capability of the sample.

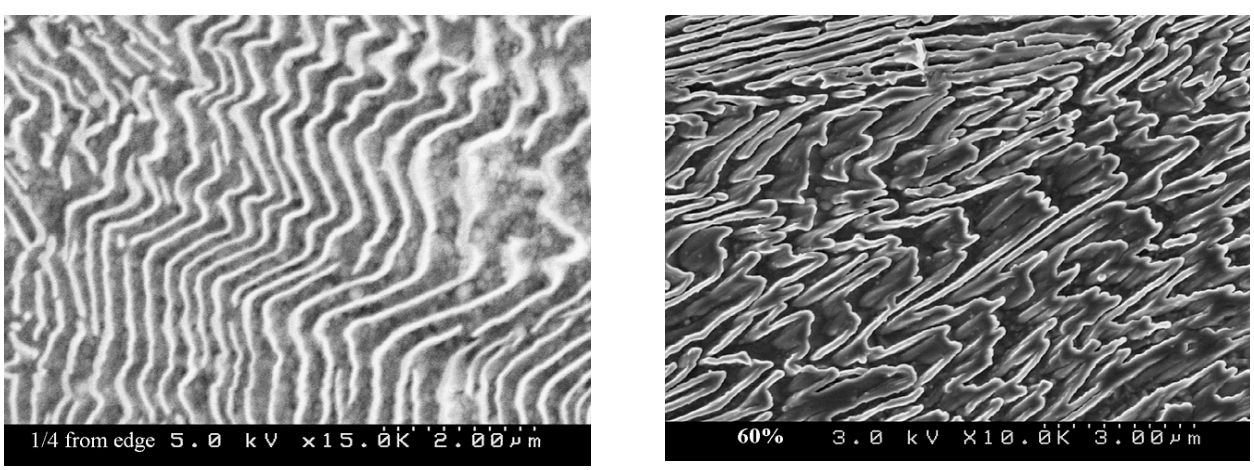

(a) (b)

Figure 3. Local instabilities in pearlite due to buckling of the carbide plates, after 0.30 strain (a) and 0.60 strain (b).

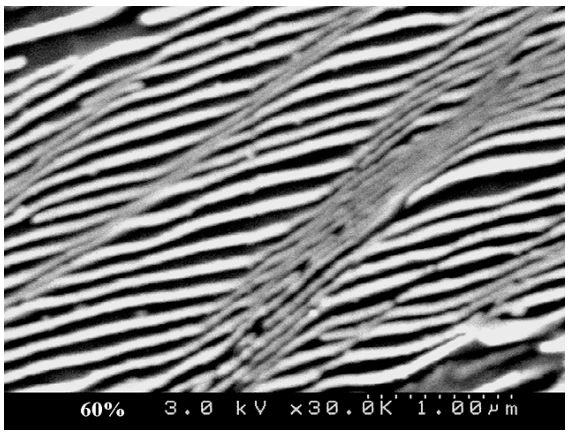

(a)

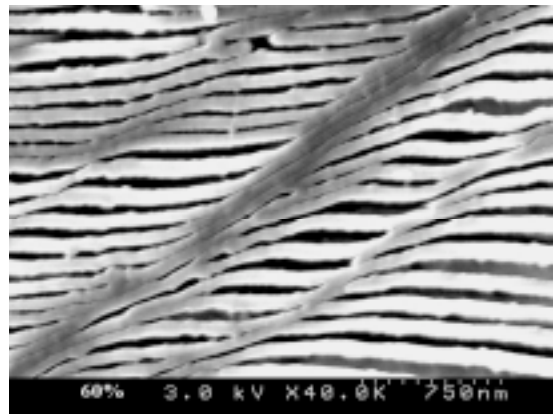

(b)

Figure 4. Localized shear of the carbide plates in pearlite after 60% strain, low magnification (a) and high magnification (b).

Kinking in pearlite plates, which were subjected to severe plastic deformation, has also been observed in steel-copper wires [11] during wire drawing. The kinking was believed to initiate in the carbide plates with the ferrite matrix "following" the kinking carbide. A similar mechanism is likely active in the pearlitic UHCS during high rate deformation. The stronger carbide is inherently expected to have a flatter stress-strain curve than the softer ferrite matrix. The flatter stress-strain curve for the carbide limits work hardening, which will encourage localization in the carbide and the development of an instability in the form of an initiating kink. Once the kink has initiated in the carbide, it will control the direction of kink propagate in the pearlite.

Failure

Examination of the shear band that led to failure in the pearlitic sample provided valuable insight into the influence of microstructure and deformation on the development of instabilities during high rate deformation. Figure 5 shows an overview of the shear band. The pearlite plates bordering the band are highly deformed and strongly oriented in the shear band direction. A graphite piece, originally oriented vertically in the photograph, was dragged into the shear band and deformed within the band. The original diameter of the graphite stringer is about 6 µm whereas the stringer in the shear band is about 2.5 µm.

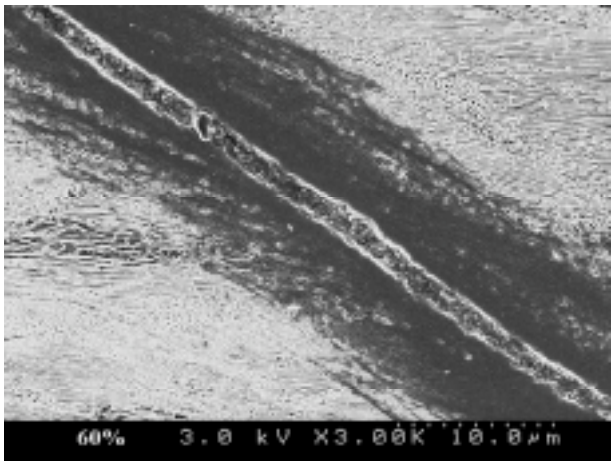

Figure 5. SEM photomicrograph of the adiabatic shear band in the pearlitic steel illustrating the fine pearlite structure adjoining the band and the graphite stringer trapped within the band.

Figure 6 shows a high magnification microstructure of the center of the shear band shown in Figure 5. A fine structure is observed with nanostructure features in the order of 70 nm. In agreement with other investigators [12-14] these features are the ferrite grain size. Adjacent to the adiabatic shear band, a mixture of two structures appears. Segmented, broken-up (ultrafine) regions are mixed with oriented pearlite regions. The lamellar spacing in the pearlite remains about the same throughout this unique region. Significantly, the spacing of the pearlite in the shear band is about the same as the pearlite spacing away from the ultra-fine structure region. This mixed structure results from the two thermal events during and after deformation - adiabatic heating resulting from the large shear strain followed by subsequent rapid cooling. The microstructure in the shear band suggests that the temperature rise exceeds the A_1 transformation temperature. Most of the pearlite will transform to face-centered-cubic austenite. If the increase in temperature is only about 100°C above the A_1 not all the pearlite will dissolve. This is the temperature range where three phases co-exist, fine-grained austenite, and ferrite-plus-cementite as undissolved pearlite [15] that results in the two mixed structures observed in Fig. 5. Upon rapid quenching at the completion of the shear-banding step, retransformation will take place. The ferrite grain size in the shear band is approximately 50 to 100 nm and the carbide particle size is believed to be approximately 1.5 nm. Nano-indentation hardness measurements gave values as high as 11.5 GPa.

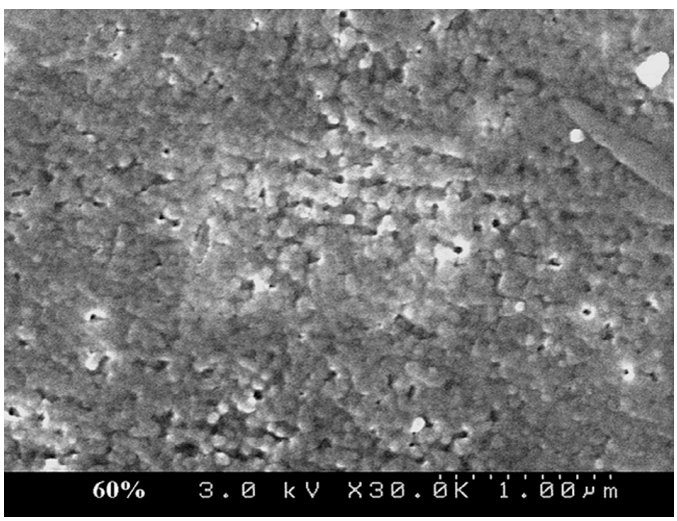

Figure 6. High magnification SEM photomicrograph illustrating the ultra fine ferrite structure in the center of band shown in Fig. 5.

Deformation in the Shear Band

Figure 7 illustrates a construction of the stress-strain-temperature history of the sample in the shear band. The initial strain region is that recorded in the Hopkinson bar test (Fig. 1). The flow stress continues to decrease to a strain of $\varepsilon = 2.8$ where the flow stress is 500 MPa. This is the flow stress of UHCS deformed at 1000 s^{-1} at 730°C [5]. A slight increase in the flow is shown at 800°C when transformation begins and austenite forms [at $\varepsilon = 3.2$]. Austenite is known to be stronger than ferrite [16]. The flow stress continues to decrease with further deformation in the austenite matrix as pearlite and cementite dissolve with increasing temperature. The flow stress decreases to 200 MPa at the end of shear band development, where the strain is $\varepsilon = 7.2$ and the final temperature is 1180°C. Rapid quenching follows since the band is bonded to a much colder matrix (i.e. 300°C).

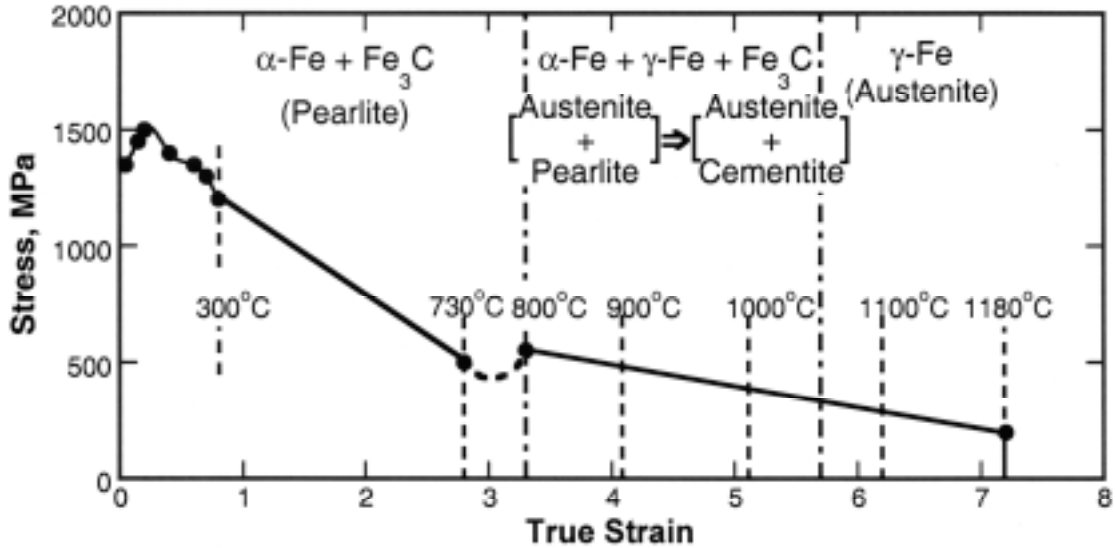

Figure 7. Stress-strain response within the shear band during high rate deformation of the UHCS-1.3C material.

The hardness of the shear band is extraordinarily high, 11.5 GPa. This is equivalent to a yield strength of 4600 MPa (667 ksi). We propose that this high strength is a result of nano-size carbides distributed uniformly in the ultra-fine ferrite grains (70 μm) [17]. This microstructure arises from a divorced eutectoid transformation (DET) that takes place during deformation in the shear band. We define the divorced eutectoid transformation as a transformation that is divorced of all normal transformations including pearlite, bainite and martensite. The structural changes are best described in three stages: (1) deformation in the ferrite range, up to $\varepsilon = 3.2$, (2) deformation in the austenite range, $\varepsilon = 3.2$ to 7.2 and (3) quenching after deformation.

In the first stage, the pearlite spacing is decreased, with simultaneous decrease in the cementite plate thickness. In addition, the carbide plates develop dislocation substructures during severe plastic deformation. The cementite layers are observed to be in the order of 1 to 5 nm for strains of about 3.0 [18, 19]. The second stage has the ferrite transforming to austenite. This transformation is athermal, i.e. instantaneous. The austenite will contain the same amount of carbon in solution as in ferrite (0.02 wt. %), because there is no time for carbon diffusion into the austenite lattice. This is because of the high strain rate in the shear band (6×10^5 s^{-1}), which produces a time in austenite of 10^{-5} s. The highly deformed carbide plates further deform in austenite and ball-up to become individual carbide particles with sizes in the order of 1-2 nm. The low-carbon austenite penetrates mechanically between the carbide particles. The third stage involves re-transformation of austenite containing nano-carbides to ferrite. The cooling rate is estimated at 10^6 °C s^{-1} [8]. The austenite to ferrite transformation is athermal, and the nano-carbides will remain fine. The ferrite may retain 0.02 wt % C. The grain size of the transformed ferrite is dependent on a number of factors. The variables that need consideration are the prior austenite grain size, the initial ferrite grain size and the amount of deformation in each phase. Multi-transformation as in deformation by ball milling leads to nano-ferrite grain sizes (less than 20 nm) [14], whereas single transformations lead to ferrite grain sizes that are over 50 nm [13].

Criteria for Initiation of Adiabatic Shear Bands

Many investigators [6, 20] have pursued the study of adiabatic shear bands. The maximum shear stress criterion is the most common approach used to explain the initiation of shear banding. This criterion states that instability in the form of adiabatic shear bands will take place when the rate of strain hardening is exceeded by the rate of thermal softening. Thus, when the maximum stress for plastic flow is reached, shear banding will start. Constitutive relations have been developed to predict the occurrence of shear bands. A common assumption is to utilize data from quasi-static tensile tests to establish a rate of strain hardening and to relate it to the rate of thermal softening from thermodynamic data to predict when shear banding will occur. These two aspects of the shear band predictive criteria, namely, using quasi-static data and a maximum shear stress criterion, have been questioned [19, 20 and 21]. It is the authors' belief that the microstructure of the steel, prior to and during deformation, are the principal factors determining the start of adiabatic shear banding. These changes are especially profound and complex in all ferritic carbon steels. These complexities are related to the intervention of strain aging during deformation. It will be shown that strain aging contributes to strain hardening that varies with strain rate and with temperature.

Figure 8 illustrates the influence of strain rate on the ultimate tensile strength of ferritic steel as a function of temperature. The data are from the extensive work of Manjoine on a 0.3 wt% C steel [21]. The ultimate tensile strength is compensated by the elastic modulus to incorporate the influence of temperature on elastic modulus as in typical constitutive relations [22-24]. Data for the UHCS-1.25%C tested at about 1000 s^{-1} is also included [5]. The pattern of strength changes with temperature and strain rate is unusual. Regions are observed where $d\sigma/dT$ is positive and where $d\sigma/dT$ is negative. Similar results are noted when Manjoine's data is plotted as the flow stress at a small strain of 2%. Meaningful constitutive laws for plastic flow of ferritic steels under high strain rate adiabatic conditions require consideration of these observations. The anomalous change of flow stress with temperature and strain rate is attributed to the increasing influence of moving carbon atoms with moving dislocations.

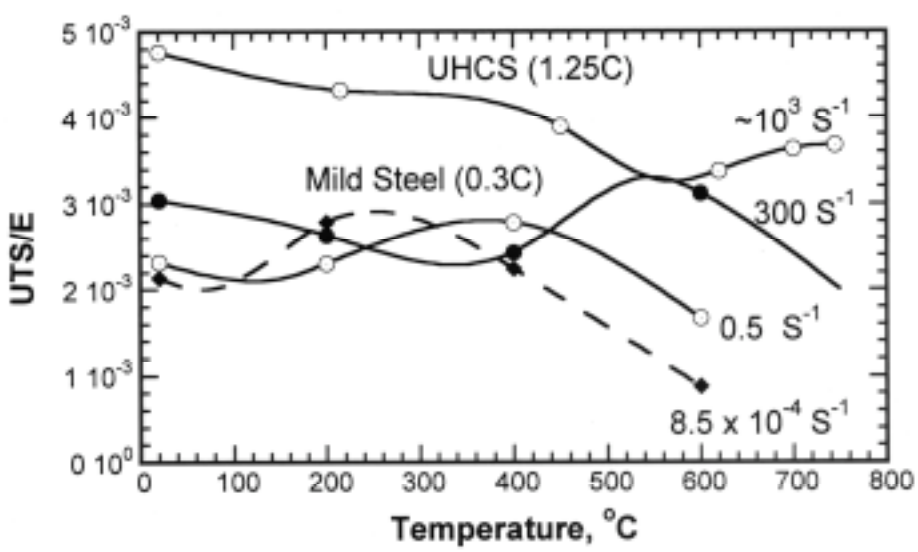

Figure 8. Elastic-modulus-compensated ultimate tensile strength versus temperature for a 0.3%C steel.

Figure 9 show true stress-true strain curves for the 0.3% C steel at room temperature for the three strain rates studied by Manjoine. The strain hardening exponent, n, in $\sigma = K\varepsilon^n$ is given in the graph. The rate of strain hardening is seen to decrease with an increase in strain rate. The strain hardening exponent, n, is decreased by a factor of 5.4 from the quasi-static strain rate (8.5×10^{-4} s^{-1}) to the dynamic strain rate of 300 s^{-1}. Analyses of the Manjoine data at temperatures above room temperature indicated changes in this ratio. It is 3.0 when calculated at 200°C, and becomes less than unity at 400°C (0.83). Since deformation at high strain rates leads to temperature rises, these changes in the strain-hardening exponent need to be considered in the application of the maximum shear stress model for adiabatic shear band formation.

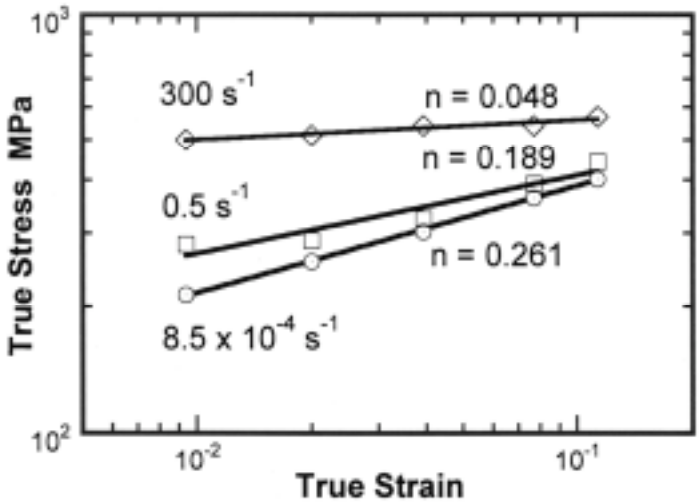

Figure 9. True stress, true strain behavior of a .3%C steel at three strain rates. Data is from the work of Manjoine.

The stress-strain curve for the pearlitic UHCS material (Figure 1) shows the maximum flow stress to occur at 0.1 strain followed by large region of strain softening with shear bands finally developing at 0.8 strain. A search of the literature reveals only limited data on the observation of large strain softening regions during high strain rate deformation. The work of Wulf [25] complements the present work with high strain rate (10^4 s^{-1}) compression tests on 4130 steel. The author showed the maximum flow stress to be reached in the order of 0.1 to 0.25 true strain followed by continued deformation to strains as high as 0.9. These observations have led us to consider another criterion for the initiation of shear bands. The model is based on the concept that it is the work of deformation in the large strain-softening region that leads to the initiation of the shear band. Thus, when the ferritic steel is deformed, its internal energy is increased in the form of lattice distortions. These include creation of dislocations, their reorganization into networks, refinement of particles that leads to increase in surface energy, point defects that lead to voids, carbon atoms that dissolve into the iron lattice, and to the increase in the vibrational energy of the material from adiabatic heating. When the strain energy in the material is build up to a value that it can no longer tolerate, it will release some of it by the formation of the shear band. This is like sudden recrystallization of a severely cold-worked material as it is heated to a temperature where new grains will form to release the stored energy of cold work.

A calculation for the critical strain energy for shear banding was made for the pearlitic UHCS material. It is equal to the work of deformation (area of the σ - ε curve to the start of shear banding). The value is 1120 MJm^{-3}. This work of deformation results in two distinctly different contributions to the energy of the material. One is the adiabatic heat produced in the sample and the other is the increase in the internal energy of the material (the latent energy). The latent energy in the band is generally believed to be a small

fraction of the total strain energy in the order of 15% [26]. It is possible to make an estimate for the case of the pearlitic UHCS material. Hardness measurements showed the 3.5 GPa hardness before testing increased to 6.5 GPa at the start of shear banding. Thus the hardness increased by a factor of 1.8. This means that the flow stress will have increased from the initial value of 1300 MPa to 2340 MPa at 0.8 strain, if adiabatic heating had not occurred. The estimated strain energy for this structural change is one-half times the incremental strain of 0.6 (from 0.2 to 0.8) times the corresponding incremental stress increase of 840 MPa (from 1500 to 2340 MPa) yielding 252 MJm^{-3}. The latent heat, therefore, represents 22% of the total strain energy. This high ratio is likely related to the remarkable way a lamellar structure deforms with straining. The true contribution to heating is less than 300°C as initially calculated.

If the initial strain energy of the UHCS material is made higher than for the pearlitic structure, for example, a martensitic structure, then less strain energy should be needed to cause shear banding. This is, in fact, the case. The UHCS sample quenched to a hardness of R_c = 63, required only 624 MJm^{-3} strain energy to form an adiabatic shear band at a strain of 0.2 [27]. Determination of the stored (latent) energy requires a knowledge of the change in structure of the material adjacent to the shear band. If the matrix hardness is reduced by strain tempering this would result in a the latent energy that is *negative*. Therefore the sample is heated to a higher temperature than that predicted from the calculated strain energy of 624 MJm^{-3}. Data on true stress – true strain response together with data on the strength changes during deformation prior to shear banding are needed to pursue the model of a strain energy criterion.

Summary and Conclusions

The mechanical response of a UHCS-1.3C, pearlitic steel during high rate compression (approximately 4000 s^{-1}) has been studied. The sample was deformed to large engineering strains (-0.55) without fracture and showed extensive ability to absorb energy. The carbide plates exhibited significant distributed kinking during deformation which results in significant amounts of energy absorption. The loss in load bearing capability was associated with the initiation and propagation of adiabatic shear bands. Localization occurred due to adiabatic shear bands, in which austenite formed. Subsequent cooling produced a divorced-eutectoid transformation, which resulted in a microstructure consisting of 50 to 100 nm sized ferrite grains. The hardness of the band is 11.5 GPa. The results show the large potential for use of UHCS in applications involving dynamic loading. A criterion for predicting the initiation of shear banding is proposed based on a critical strain energy concept rather than the maximum shear stress model.

References

[1] D. R. Lesuer, C. K. Syn, A. Goldberg, J, Wadsworth and O. D. Sherby, JOM, 45 (8) (1993), 40.
[2] C. K. Syn, D. R. Lesuer and O. D. Sherby, *Metallurgical Transactions,* 25A (1994), 1481.
[3] E.M. Taleff, C.K. Syn, D.R. Lesuer and O.D. Sherby, , *Metallurgical and Materials Transactions,* 27A (1995), 111.
[4] D.R. Lesuer, C. K. Syn and O. D. Sherby, *Acta Metallurgica and Materialia*, 43 (10) (1995), 3827.

[5] Z. Rosenberg, D. Dawicke and S. Bless,: in *Metallurgical Applications of Shock-Wave and High-Strain-Rate Phenomena*, Marcel Decker, New York, (1986) 543.
[6] Y. Bai and B. Dodd, Adiabatic Shear Localization, Pergamon Press, New York (1992).
[7] C. Zener and J. H. Hollomon, *Journal of Applied Physics*, 15 (1944), 31.
[8] C. L. Wittman, M. A. Meyers and H-r Pak, Metallurgical Transactions, 21A (1990), 707.
[9] M. Umemoto, S. Hau, T. Yasuda and K. Tsuchiya, Materials Transactions, 43 (2002), 2536.
[11] W. Grunberger, M. Heilmaier and L. Schultz, *Materals Science and Engineering*, A303 (2001), 127.
[12] J. Languillaume, G. Kapelski and B. Baudelet, *Acta Materialia*, 45 (1997), 1201.
[13] M. Umemoto, *Materials Transactions,* 44 (2003), 1900.
[14] M. Umemoto, Z. G. Liu, K. Masuyama, X. Hao, K. Tsuchiya. *Scripta Materiala,* 44 (2001),1741.
[15] O.D. Sherby and T. Oyama, U.S. Patent 4,533,390, Aug. 6, 1985.
[16] D. R. Lesuer, C. K. Syn, J. D. Whittenberger, M. Carsi, O. A. Ruano and O. D. Sherby, *Materials Science and Engineering*, A317 (2001), 101.
[17] C.K. Syn D. R. Lesuer and O. D., Sherby, submitted to *Materials Science and Technology,* (2004).
[18] G. Langford, *Metallurgical Transactions*, 1 (1970), 465.
[19] G. D. Smith, D.A. Smith, K. E. Easterling. Proc. 3rd Int'l Conf. The Strength of Metals and Alloys, Inst. Metals and Iron and Steel Inst., Cambridge, England, (Aug 20-25, 1973), 75.
[20] T. W. Wright, The Physics and Mathematics of Adiabatic Shear Bands, Cambridge University Press, Cambridge, UK (2002).
[21] M.J. Manjoine, Journal of Applied Mechanics, 12 (1944), A211.
[22] J. F. Mescall and H. Rogers, in "Innovations in Ultrahigh Strength Steels Technology", G. Olsen, m. Azrin and E.S. Wright, editors, Sagamore Army Materials Research Conference, Lake George NY, 34 (1987), 287-314.
[23] J.G. Cowie, M. Azrin and G.B. Olsen, in "Innovations in Ultrahigh Strength Steels Technology", G. Olsen, m. Azrin and E.S. Wright, editors, Sagamore Army Materials Research Conference, Lake George NY, 34 (1987), 357-381.
[24] S. L. Semiatin, M. R. Staker and J. J. Jonas, "Plastic Instability and Flow Localization in Shear at High Rates of Deformation, *Acta Metall*., 32 (9) (1984), 1347-1354.
[25] G.L. Wulf, "The High Strain Rate Compression of 1023 and 4130 Steels", Int. J. Mech. Sci., 30 (1978), 843-848.
[26] G.I. Taylor and H. Quinney, Proceedings of the Royal Society, 143 (1931) 307.
[27] D. R. Lesuer, C. K. Syn, O. D. Sherby, D. W. Kum, "High Strain Rate – High Strain Response of an Ultrahigh Carbon Steel Containing 1.3%C and 3% Si", *Materials Science Forum*, (2003), 841-846.

Acknowledgments

This work was performed under the auspices of the U. S. Department of Energy by the University of California, Lawrence Livermore National Laboratory under Contract No. W-7405-Eng-48. The authors are indebted to Mary Leblanc for the split Hopkinson pressure bar tests.